Video Article

In Vivo Quantitative Assessment of Myocardial Structure, Function, Perfusion and Viability Using Cardiac Micro-computed Tomography

Elza van Deel[1,2], Yanto Ridwan[1], J. Nicole van Vliet[1], Sasha Belenkov[3], Jeroen Essers[1,4,5]

[1]Department of Genetics, Erasmus MC, Rotterdam

[2]Department of Experimental Cardiology, Erasmus MC, Rotterdam

[3]PerkinElmer, Inc.

[4]Department of Vascular Surgery, Erasmus MC, Rotterdam

[5]Department of Radiation Oncology, Erasmus MC, Rotterdam

Correspondence to: Jeroen Essers at j.essers@erasmusmc.nl

URL: http://www.jove.com/video/53603
DOI: doi:10.3791/53603

Keywords: Bioengineering, Issue 108, Imaging, mouse cardiac functional imaging, LV function, cardiovascular function, perfusion imaging, myocardial infarction, ischemia, LAD artery occlusion, MicroCT, Quantum FX, contrast agent, eXIA160

Date Published: 2/16/2016

Citation: van Deel, E., Ridwan, Y., van Vliet, J.N., Belenkov, S., Essers, J. *In Vivo* Quantitative Assessment of Myocardial Structure, Function, Perfusion and Viability Using Cardiac Micro-computed Tomography. *J. Vis. Exp.* (108), e53603, doi:10.3791/53603 (2016).

Abstract

The use of Micro-Computed Tomography (MicroCT) for *in vivo* studies of small animals as models of human disease has risen tremendously due to the fact that MicroCT provides quantitative high-resolution three-dimensional (3D) anatomical data non-destructively and longitudinally. Most importantly, with the development of a novel preclinical iodinated contrast agent called eXIA160, functional and metabolic assessment of the heart became possible. However, prior to the advent of commercial MicroCT scanners equipped with X-ray flat-panel detector technology and easy-to-use cardio-respiratory gating, preclinical studies of cardiovascular disease (CVD) in small animals required a MicroCT technologist with advanced skills, and thus were impractical for widespread implementation. The goal of this work is to provide a practical guide to the use of the high-speed Quantum FX MicroCT system for comprehensive determination of myocardial global and regional function along with assessment of myocardial perfusion, metabolism and viability in healthy mice and in a cardiac ischemia mouse model induced by permanent occlusion of the left anterior descending coronary artery (LAD).

Video Link

The video component of this article can be found at http://www.jove.com/video/53603/

Introduction

Ischemic heart disease (IHD) continues to be the single greatest cause of morbidity and mortality for men and women worldwide[1]. Because of complexities and interrelationships that exist between the organs and systems at the organismal level, the use of the whole animal as a model of IHD remains relevant not only for our better understanding of disease pathophysiology, but also permitting evaluation of novel preventive and therapeutic strategies. Mouse models, in particular, have contributed to our knowledge of cardiac development, pathogenesis of myocardial infarction, myocardial hypertrophy, myocarditis, and aneurysmal lesions[2-7]. The parameters that determine cardiac performance and are useful in terms of prognosis and choice of therapeutic intervention are cardiac mass and geometry, global and regional function, spatial distribution of myocardial blood flow and myocardial viability.

However, most of traditional investigational methods used in mouse models of heart disease involve invasive measurements that require hours for completion, thus the animal can't be used for repeat measurements, or the method will require animal sacrifice[8-12]. For example, to measure regional myocardial perfusion, radioactively or fluorescently labeled microspheres are used where radioactive count or fluorescent signals are detected on a physically dissected heart or *in situ*[13,14].

Similarly, evaluation of infarct size in animal models of myocardial infarction is most commonly performed by triphenyltetrazolium chloride (TTC) staining, and in order to determine the time course of infarct evolution and the effect of therapeutic interventions, this technique requires that the animals need to be sacrificed for heart histopathological examination at various time points[15]. As such, non-destructive and humane techniques that would allow quantitative and longitudinal analysis of cardiac morphology, function, metabolism and viability are of paramount importance. In this context, preclinical imaging is of great relevance. Among the currently available imaging modalities magnetic resonance imaging (MRI) and echocardiography are the most commonly used[16,17,18].

However, and despite the fact that MRI is considered the modality of reference in both clinical and preclinical work, the high cost to acquire and maintain dedicated small-animal MRI systems, as well as the complexity of this technology for non-advanced users to operate, make MRI prohibitively expensive for routine use. With regards to echocardiography, there exist significant disadvantages to the way cardiac function is measured. The data produced by most echocardiographic examinations are two-dimensional, and in order to derive volumes, geometrical

assumptions need to be made[19]. In addition, poor intra- and inter-observer reproducibility is another significant limitation of this technique. Radioisotope imaging with single photon emission computed tomography (SPECT) and positron emission tomography (PET) are predominantly used for assessment of myocardial perfusion and metabolism[17,20,21]. However, restricted spatial resolution of these imaging modalities makes cardiac imaging in mice challenging.

On the other hand, with the advent of flat panel detector technology that allows better X-ray sensitivity and faster readout times, current state of the art MicroCT systems can now provide cardio-respiratory gated three-dimensional (3D) and four-dimensional (4D) images of MRI-grade quality. They are virtually maintenance cost free and easy to operate by non-advanced users. Thus, such MicroCT instruments can be well suited for routine examination of small animals as models of human disease. Most importantly, with the development of a novel preclinical iodinated contrast agent, simultaneous functional and metabolic assessment of the heart became possible[22-24].

This contrast agent contains a high concentration of iodine (160 mg/ml), producing strong blood-pool contrast after its intravenous administration enabling *in vivo* imaging of vasculature and the heart chambers. Within an hour after administration, a continual increase in myocardial contrast associated with its metabolic uptake can be observed, thus the same contrast agent can be used for evaluation of myocardial stunning and viability.

The goal of the technique outlined in this manuscript is to enable researchers to use the high-speed MicroCT system with intrinsic cardio-respiratory gating, in conjunction with blood-pool iodinated contrast agent, for determining myocardial global and regional function along with myocardial perfusion and viability in healthy mice and in a cardiac ischemia mouse model induced by permanent occlusion of the left anterior descending coronary artery (LAD). By using this animal model and imaging technique, rapid evaluation of the most important cardiac parameters can be performed repetitively with a single imaging modality and without the need for invasive procedures or the need to sacrifice the animals. The technique can be performed to evaluate novel preventive and therapeutic strategies.

Protocol

All animal work in this study was approved by the Erasmus MC animal research ethics committee. Throughout the experiments, the animals were kept in accordance with Erasmus MC institutional regulations. At the end of the experiment animals were euthanized using an overdose of inhalant anesthetic isoflurane. Please seek institutional animal care and use committee approval before commencing this work.

1. Preparation of Cardiac Ischemia Model

1. Anesthetize the mouse (C57Bl6, 12 weeks old) by inhalation of 4% isoflurane. Intubate the animal using a 20 G cannula and respirate the mouse at 100 breaths per minute with a peak inspiratory pressure of 18 cm H_2O and a positive end expiratory pressure of 4 cm H_2O.
    1. Use a gas mixture of O_2/N_2 (v/v = 1/2) containing 2.5% isoflurane to maintain anesthesia and apply eye drops to prevent desiccation of the eyes while under anesthesia. Place the mouse on a heating pad and measure body temperature rectally to maintain body temperature at 37 °C during surgery.
2. Inject buprenorphine (0.05-0.2 mg/kg) subcutaneously just prior to surgery and check the toe pinch reflex to assure sufficient depth of anesthesia before the start of the surgical procedure. Depilate the mouse chest using hair removal cream and apply iodine to the skin.
3. Perform an incision by making a small cut with scissors in the skin between the 2nd and 3rd left ribs. Pull the pectoralis minor and the xiphihumeralis muscle as well as the latissimus dorsi muscle to the side using small hooks to allow access to the intercostal muscles.
4. Carefully cut through the 3rd intercostal muscle without harming the lungs using a curved 2 mm blade spring scissor. Push the lung aside using a small piece of wet gauze and rupture the pericardium.
   NOTE: Be careful not to damage the left phrenic nerve.
    1. Reposition the small hooks that hold the muscle to inside the thorax and reposition them so that a large part of the left ventricular (LV) free wall and part of the left atrium are visible.
5. Insert a 7-0 silk surgical suture underneath the left coronary artery and occlude the artery by firmly knotting the suture.
   NOTE: Because in most mice the coronary artery is not visible, determine the position of the ligature using the atrium and always ligate the coronary artery 2 mm below the edge of the left atrium in order to standardize infarct size.
6. Visually check for successful induction of the infarct by confirming the paling of the left ventricular free wall. When paling is not observed, perform an additional attempt to occlude the LAD.
7. Close the chest firmly using a 6-0 silk surgical suture.
   NOTE: The chest should be closed airtight to allow independent breathing after recovery.
8. Clean the wound with saline and close the skin using silk sutures. Apply wound spray on the skin to stimulate wound healing and prevent infection.
9. Turn the isoflurane off and wait until the animal start to breathe by itself before removing the ventilation tube. Place the mouse in a cage on a heating pad while recovering.
   NOTE: Do not leave an animal unattended until it has regained sufficient consciousness to maintain ventral recumbency. Do not return an animal that has undergone surgery to the company of other animals until fully recovered.
10. Administer additional doses of buprenorphine every 8-12 hr after surgery for post-surgery analgesia. Administer Buprenorphine (50 µg/kg) intraperitoneally.
    NOTE: Scan the animals by MicroCT (Section 3) 3-4 hr after the surgery for the first scan and 6-7 hr after the surgery for the second scan.

2. Injection of MicroCT Contrast

1. In order to acquire anatomic, functional, and metabolic information in two successive MicroCT imaging sessions, use iodinated contrast agent.

2. Expose and treat the rubber of the vial stopper using 70% alcohol. Using a low dead space syringe, withdraw a required volume (5-10 µl/g of body weight) of the contrast agent. To prevent the risk of embolism during injection, purge air bubbles, if any, by advancing the plunger back and forth and/or gently tapping the side of the syringe and slowly expelling the air into sterile absorbent tissue until fluid appears at the tip of the needle.
   Note: Injection of the MicroCT contrast can be performed in conscious or sedated animals. Physical restraint should be performed on conscious animals. To minimize stress, consider light sedation or general isoflurane anesthesia with an inhalation anesthesia system.
3. Prior to injection, swab the tail with 70% alcohol. Warm up the tail with a lamp or by immersing the tail into warm water (40-45 °C) to provide better vessel dilation. Inject the contrast agent intravenously (*e.g.* via one of the lateral tail veins) at 5-10 µl/g of body weight.
   Note: Optimize the injected dose for a particular animal model or MicroCT instrument's acquisition settings, as the contrast enhancement can be influenced by the health or dietary status of the animal under study and the level of image noise.

3. MicroCT Imaging

1. Prior to contrast injection, turn on MicroCT scanner by pressing the computer power button. Start the MicroCT control software, and warm up the X-ray tube by clicking the Warm-up button shown in the software control window.
2. Allow for the Live Mode button to appear in the control software indicating that warm-up is complete. Insert the small bore cover and place the small animal bed.
3. Create or select the appropriate database, study, and subject where the image data will be saved. To create a new database click the New Database button in the Database window, enter a name that would specify the new database, click Browse button in the dialog box that appears, navigate to the drive where the database will be saved, and click OK. Observe the new database in the Database window. To connect to an existing database, click the Connect to Database button in the Database window, and double-click the database name.
4. Set the scan conditions by selecting the following parameters from the drop-down menus of the software control window: X-ray tube voltage, 90 kV; CT X-ray tube current, 160 µA; Live X-ray tube current, 80 µA; FOV, 20 mm; Gating technique, cardio-respiratory; Scan technique, 4.5 min.
   NOTE: This imaging protocol allows for reconstruction of end-diastolic and end-systolic 3D datasets, each with a matrix size of 512 x 512 x 512, with a reconstructed isotropic voxel size of 40 µm.
5. After injecting the animal with the contrast agent, anesthetize it in an induction chamber by inhalation of 4% isoflurane. Place the animal on the animal bed of the scanner with a nose cone supplying 1.5-2.0% isoflurane in an air oxygen mixture. If necessary, adjust the flow of isoflurane to achieve the animal's stable respiratory activity with ≤60 breaths per minute.
6. Close the instruments door by sliding it to the right to engage the safety interlock. Turn on Live Mode by clicking the Live Mode button shown on the control software window to view the subject in real time. Observe the X-capture window and the animal.
   Note: The instrument does not generate X-rays unless the door is properly closed and the safety interlock is engaged.
7. Move the animal bed to align the mouse chest within the field of view (FOV) by pressing the stage Z-axis control back and forth buttons located on the front panel of the instrument. Verify that the chest is in the center within the FOV. Use the animal bed control LEFT and RIGHT arrows located on the front panel of the instrument to position the animal inside the blue bounding box.
   1. Rotate the gantry by selecting "90" from the Rotation Control drop-down list shown on the control software window and clicking the Set button. Make sure the animal remains within the blue bounding box of the X-capture window. If necessary, align the animal by using the animal bed control UP and DOWN arrows located on the front panel of the instrument.
      Note: Only the image data inside the blue bounding box shown on the X-capture window will be used to reconstruct the 3D volume.

8. In the Xcapture window, resize the cardio-respiratory region of interest (ROI) with the left mouse click and by dragging the ROI edges with the mouse cursor, so that the cardio-respiratory traces are clearly visible in the synchronization view. Ensure that the ROI covers the diaphragm and the apical portion of the heart in all gantry positions. Rotate the gantry 90° as described in step 3.6 to make sure that the cardio-respiratory traces are still clearly visible.
   NOTE: In order to prevent unnecessary exposure to ionizing radiation, minimize the time during which the animal position and cardio-respiratory ROI are adjusted.
9. Click the CT Scan button shown on the control software window to initialize the acquisition. CT Scan Confirmation Message will appear. Click the YES button shown in the CT Scan Confirmation Message to confirm. Click the NO button to abort the scan. Once the YES button is pressed, the red X-ray energizing indication located on the instrument will be lit.
   NOTE: The indication will be also visible by the blinking voltage icon of the instrument status box of the control software window. The scan will be completed in 4.5 min. The X-ray tube will be switched off automatically and the red X-ray energizing indication located on the instrument and on the control panel of the control software window will dim. The projections will be automatically sorted and the progress will be indicated by the green progress bars shown on GetSynchronizedRaw window. The volume sets representing end-diastolic and end-systolic phases of the cardiac cycle will be automatically reconstructed within 2-3 additional min.
   NOTE: To abort the scan click the emergency stop button in the Control panel of the control software window or push the mechanical emergency stop button located on the front panel of the instrument.
10. Observe the transaxial, coronal, and sagittal views of the reconstructions in 2D Viewer software. Take a few seconds to review the quality of the acquired images. Look for the signs of animal movement that can be caused by an inadequate level of anesthesia. If necessary, make appropriate modifications and repeat the scan.
    NOTE: If the structures in the image are doubled, shown with double edges, or shown with streaks, then these are the usual "red flags" that can indicate that the level of anesthesia may be inadequate and that the animal has moved during the scan. In such instances, the level of anesthesia should be adjusted and the scan should be re-acquired.
11. Remove the animal from the scanner and allow for full recovery from anesthesia under supervision.
12. Acquire an additional MicroCT scan during the metabolic phase of the contrast uptake (3 to 6 hr after the contrast injection).
    NOTE: More details on mean myocardial enhancement values for C57Bl/6 and BALB/c mice were published by Detombe et al and Ashton *et al.*[22,23].

4. MicroCT Data Analysis

1. Load both end-diastolic and end-systolic VOX files into Analyze 12 software.
2. Open each loaded image with the Oblique Sections module and perform short-axial image reformation.
3. In order to minimize image-processing time consider cropping the images using the Subregion/pad volume function of the Image Calculator module. For both volumes, maintain identical SubRegion Low and High X, Y, Z dimensions.
4. Append both volumes and open with the Volume Edit module. For better visualization of the structures, adjust image intensity if necessary.
5. Perform endocardial contour segmentation. From the Semi-Automatic tab of the Volume Edit module select Object Extractor, set a seed point into the left ventricle (LV) and adjust threshold values, so that the left ventricular cavity is delineated from the myocardium. To determine the threshold value, use automatic thresholding algorithms or the full width half max value (FWHM) determined with the Line Profile module.
    1. Draw a limit along the mitral valve leaflet plane to prevent the region spreading to the aorta, click the Extract Object button to complete the segmentation. Both end-diastolic and end-systolic volumes will be processed automatically. Name the region (*e.g.* LV Cavity) and save the object map to the corresponding file directory.
6. Perform epicardial contour segmentation. Add a new object and perform the segmentation of the epicardial heart surface using either Semi-Automatic or Manual segmentation tools of the Volume Edit module. Make sure that both end-diastolic and end-systolic contours are correctly identified. If necessary, perform manual adjustment. Name the regions (*e.g.* LV Myocardium) and save the object map to the corresponding file directory.
   Note: Image filtering with the Spatial Filters module can be additionally performed to improve the speed and quality of the segmentations.
7. In order to extract volumetric measurements from the object maps (saved) open the appended volume with the Region of Interest module. Make sure the corrected map is loaded, open the sample Option window, make sure both LV Cavity and LV Myocardium objects are selected, and click the Sample Images button. Save the log file.
8. For regional analysis of the heart function and metabolism, use the Radial Divider tool of the Region of Interest module to further subdivide the segmented volumes.

5. Computation of the Global and Regional Heart Parameters

1. To compute the left ventricular stroke volume (LVSV), subtract the left ventricular end-systolic volume (LVESV) from the left ventricular end-diastolic volume (LVEDV):
   LVSV = LVEDV - LVESV;
2. To compute the left ventricular ejection fraction (LVEF), divide the left ventricular stroke volume (LVSV) by the left ventricular end-diastolic volume (LVEDV) and multiply by 100%:
   LVEF = LVSV / LVEDV*100%;
3. To compute cardiac output (CO), multiply the left ventricular stroke volume (LVSV) by the heart rate (HR):
   CO = LVSV * HR;
4. To compute the left ventricular myocardial mass (LVMM), subtract the left ventricular myocardial wall volume bound by the endocardial surface ($LVMV_{ENDO}$) from the left ventricular myocardial wall volume bound by the epicardial surface ($LVMV_{EPI}$), and multiply by the specific gravity of the myocardium, 1.05 g/cm^3:
   $LVMM = (LVMV_{EPI} - LVMV_{ENDO}) * 1.05$;
5. To compute the left ventricular myocardial mass index (LVMMI), divide the left ventricular myocardial mass (LVMM) by the mouse body weight (BW):
   LVMMI=LVMM / BW;
6. To compute the percentage of the left ventricular myocardial infarct size (%LVMIS), divide the left ventricular volume of infarcted myocardium ($LVMV_{MI}$) by the total left ventricular myocardial volume ($LVMV_{TOTAL}$), and multiply by 100%:
   $\%LVMIS = LVMV_{MI} / LVMV_{TOTAL} * 100\%$;
   Note: For LVMM, LVMMI, and %LVMIS calculations, use endo- and epicardial volume measurements from the corresponding end-diastolic or end-systolic datasets. Report average end-systolic and end-diastolic indices.
7. To compute the segmental left ventricular wall motion abnormalities (LVWM), subtract the segmental left ventricular end-systolic wall diameter (LVESWD) from the segmental left ventricular end-diastolic wall diameter (LVEDWD):
   LVWM = LVEDWD - LVESWD;
   Display the results as circumferential polar maps (Bulls eye polar plots).
8. To compute the segmental left ventricular wall thickening (%LVWTh), subtract the segmental left ventricular end-diastolic wall thickness (LVEDWTh) from the segmental left ventricular end-systolic wall thickness (LVESWTh), divide by the segmental left ventricular end-diastolic wall thickness (LVEDWTh), and multiply by 100%:
   %LVWTh = (LVESWTh - LVEDWTh) / LVEDWTh * 100%;
   Display the results as circumferential polar maps (Bulls eye polar plots).
9. To calculate the regional ejection fraction (%rEF), subtract the square of segmental left ventricular end-systolic wall diameter (LVESWD) from the square of segmental left ventricular end-diastolic wall diameter (LVEDWD), divide by the square of segmental left ventricular end-diastolic wall diameter (LVEDWD), and multiply by 100%:
   $\%rEF = (LVEDWD^2 - LVESWD^2) / LVEDWD^2 * 100\%$;
   Display the results as circumferential polar maps (Bulls eye polar plots).
10. To present regional myocardial perfusion and contrast uptake, convert the mean intensity values into CT numbers (Hounsfield units, HU). Convert both end-diastolic and end-systolic datasets by rescaling air selected from the region selected outside the animal to - 1000 HU, and water to 0 HU using a water-filled small radio-transparent tube. Display the results as circumferential polar maps (Bulls eye polar plots).

6. Statistical Analysis

1. Represent all polar plot display data as mean ± standard deviation (SD). Assess the statistical difference using one-way analysis of variance (ANOVA) or another appropriate technique.

Representative Results

MicroCT Acquisition, Image Reconstruction, and Image Quality Assessment.

Four C57Bl/6 mice, three with permanent LAD occlusion and one sham-operated, successfully recovered from the surgery and completed the imaging protocol which consisted of a single contrast agent intravenous bolus administration and two 4.5-min cardio-respiratory MicroCT acquisitions. The mean heart rate during the MicroCT studies was 385 ± 18 beats per minute. End-diastolic and end-systolic image reconstruction used proprietary intrinsic image-based gating, in which dedicated respiratory and cardiac monitoring devices such as ECG leads and respiratory pneumatic sensor were not needed. Following the reconstruction, image quality of both end-diastolic and end-systolic datasets was previewed using 2D viewer software. The image quality was found satisfactory and there was no need to perform additional image acquisitions. Thus, all the reported data were derived from two scans per mouse; the first scan taken 10 minutes post injection during the blood pool phase of the contrast, and the second scan acquired 3-4 hours post injection during the metabolic uptake phase of the contrast. Representative blood-pool short-axial end-diastolic and end-systolic cross-sections of a mouse heart with myocardial infarction (**Figure 1**) and of a mouse heart without myocardial infarction (**Figure 2**) demonstrated excellent left ventricular cavity delineation with little background noise, allowing for accurate anatomical and functional evaluation. Areas of contrast rarefaction corresponding to myocardial infarction were well demarcated on short-axial images of the mouse heart subjected to the LAD coronary artery ligation (**Figure 1**), but not in the sham-operate animal (**Figure 2**).

Quantitative Assessment of Left Ventricular Function.

Threshold-based 3D segmentations were performed on both end-diastolic and end-systolic volumes to determine left ventricular end-diastolic volume (LVEDV) and left ventricular end-systolic volume (LVESV) in each animal. Left ventricular stroke volume (LVSV), left ventricular ejection fraction (LVEF), and cardiac output (CO) were calculated from LVEDV and LVESV according to the formulas described in Section 5. The results of volume and global functional measurements are summarized in **Table 1**. Three hours after the ligation, the normalized for the animal body weight mean LVEDV was not different between the myocardial infarction group and the sham-operated animal (2.8 ± 0.23 vs. 2.3). However, the body weight normalized mean LVESV was higher in the myocardial infarction group (2.1 ± 0.31 vs. 0.92). Correspondingly, the mean LVEF and cardiac output (CO) in mice with LAD coronary artery occlusion were lower when compared to the sham-operated mouse (23.1% ± 7.1% vs. 60.5%, and 4.23 ± 0.4 ml/min vs. 13.84 ml/min respectively).

Quantitative Assessment of LV Myocardial Mass and Infarction Size.

Both left ventricular myocardial mass (LVMM) and left ventricular myocardial mass index (LVMMI) were determined based on epicardial and endocardial segmentations including papillary muscles and trabeculae. Both end-diastolic and end-systolic reconstructions were processed and the values for both myocardial infarction group and the sham-operated animal are summarized in **Table 1**. Myocardial infarct volumes were determined based on contrast rarefaction using threshold-based 3D volumetry. As shown in **Table 1**, three hours after LAD coronary artery ligation the areas at risk (AAR) in mouse 1, 2, and 3 were 22.4 %, 13.3%, and 15.8% of the LVMM respectively.

Myocardial Perfusion Imaging (MPI).

Representative end-diastolic and end-systolic circumferential polar plot displays (Bulls Eye polar plots) of myocardial perfusion in a mouse with myocardial infarction (Mouse 1) and a mouse without myocardial infarction (Mouse 4) are shown in **Figures 3** and **4**. The images used to produce the plots were acquired 10 minutes after the contrast agent administration and 3 hours after the LAD ligation. The end-diastolic and end-systolic homosegmental values obtained from the same animal were not different. However, hypoenhancement was observed in mid-anterior, mid-inferolateral, mid-anterolateral, apical anterior, and apical lateral segments of a mouse with myocardial infarction, demonstrating impairments in coronary blood flow caused by LAD artery occlusion (**Figure 3**). No such impairment could be observed in the heart of the sham-operated animal (**Figure 4**).

Myocardial Viability and Metabolism.

Representative end-diastolic and end-systolic circumferential polar plot displays (Bulls Eye polar plots) of myocardial metabolic uptake in a mouse with myocardial infarction (Mouse 1) and a mouse without myocardial infarction (Mouse 4) are shown in **Figures 7** and **8**. The images used to produce the plots were acquired 3-4 hours after contrast administration and 5-6 hours after the LAD ligation. Dissimilar myocardial contrast uptake could be also visually observed in short-axial cross-sections of a mouse heart that underwent LAD coronary artery occlusion (**Figure 5**), but not in the sham-operated mouse (**Figure 6**). The end-diastolic and end-systolic homo-segmental values obtained from the same animal were not different. The circumferential polar plots showed segment-specific abnormalities (**Figure 7**) with similar pattern to those shown on the myocardial perfusion maps (**Figure 2**). No contrast uptake defects were seen on the circumferential polar plots of the sham-operated mouse (**Figure 8**).

Quantitative Assessment of LV Regional Function.

The image quality was satisfactory to perform visual assessment of left ventricular motion and thickening from end-diastolic and end-systolic reconstructions in all imaged mice. The LV wall motion, thickening and regional ejection fraction scores for each segment of a mouse with and without myocardial infarction are given in **Figure 9** and **Figure 10**. As was expected, the LAD coronary artery ligation resulted in marked decrease of LV regional functional indices (**Figure 9**), whereas no effect was observed in the sham-operated mouse (**Figure 10**).

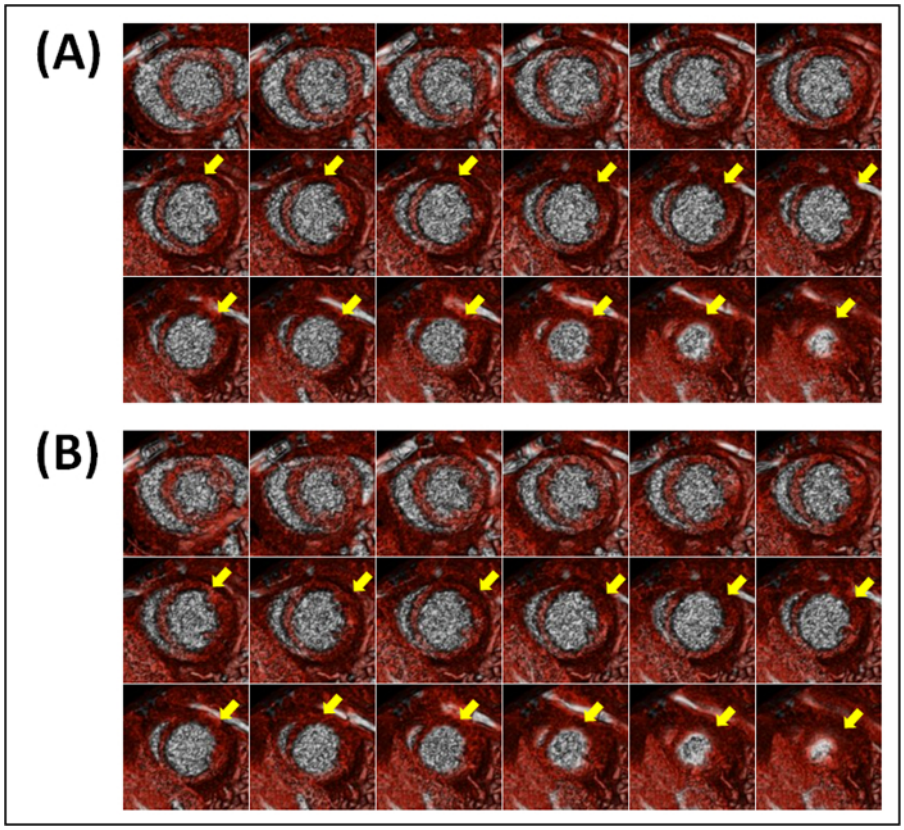

Figure 1. Representative blood-pool short-axial end-diastolic (**A**) and end-systolic (**B**) cross-sections of a mouse heart with myocardial infarction (Mouse 1). Images were acquired 3 hours after LAD coronary artery occlusion and 10 min after contrast administration. The negative contrast noted by yellow arrows is due to lack of contrast opacification in the infarcted region.

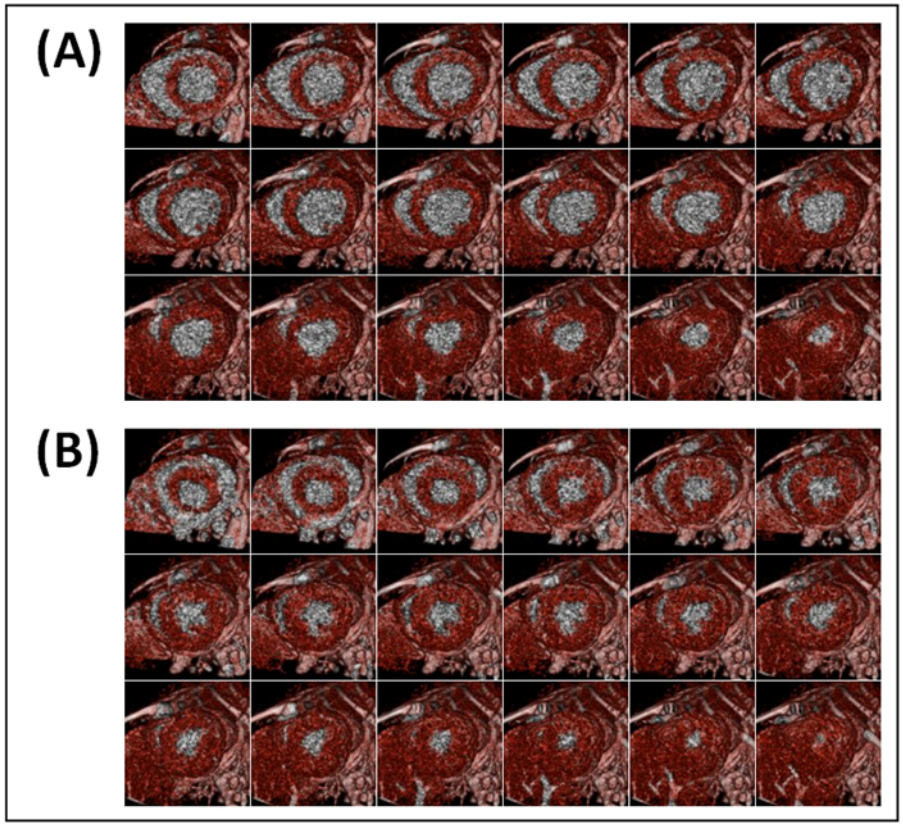

Figure 2. Representative blood-pool short-axial end-diastolic (**A**) and end-systolic (**B**) cross-sections of a mouse heart without myocardial infarction (Mouse 4). Images were acquired 3 hr after sham-operation and 10 min after contrast administration. Contrast opacification is uniformly present in all myocardial slices.

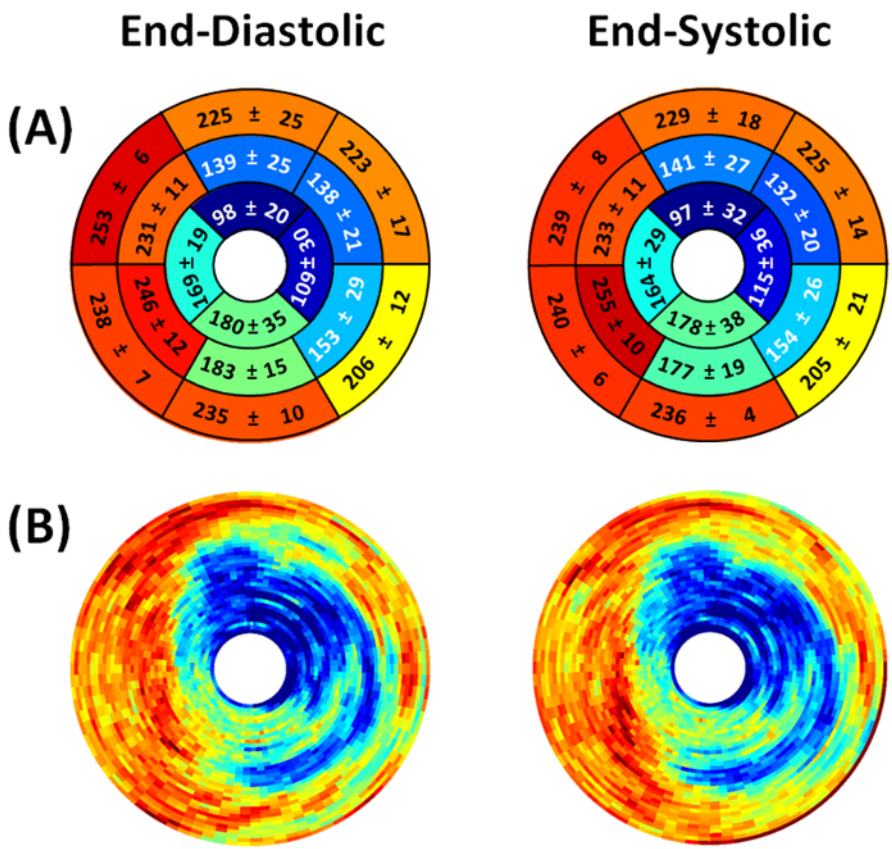

Figure 3. Representative end-diastolic and end-systolic circumferential polar plot displays (Bulls Eye polar plots) of myocardial perfusion in a mouse with myocardial infarction (Mouse 1). (**A**) The left ventricle is subdivided into basal, mid-cavity, and apical short-axial portions according to the 17-segment AHA model[25]. Dissimilar perfusion is clearly visible in mid-anterior, mid-inferolateral, mid-anterolateral, apical anterior, and apical lateral segments. Values shown represent the segmental means in Hounsfield units ± standard deviations. (**B**) Myocardial perfusion maps are shown without subdivision into 17 segments. The center of the plot corresponding to the cardiac apex (segment 17) is not shown.

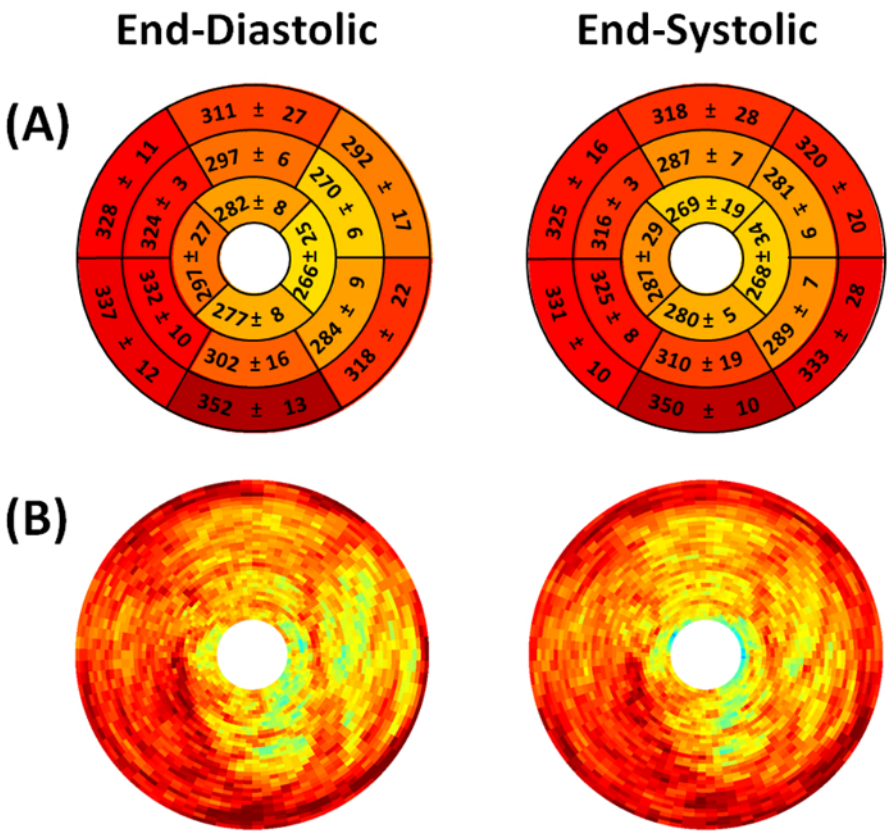

Figure 4. Representative end-diastolic and end-systolic circumferential polar plot displays (Bulls Eye polar plots) of myocardial perfusion in a mouse without myocardial infarction (Mouse 4). (**A**) The left ventricle is subdivided into basal, mid-cavity, and apical short-axial portions according to the 17-segment AHA model[25]. Similar perfusion is present in all segments. Values shown represent the segmental means in Hounsfield units ± standard deviations. (**B**) Myocardial perfusion maps are shown without subdivision into 17 segments. The center of the plot corresponding to the cardiac apex (segment 17) is not shown.

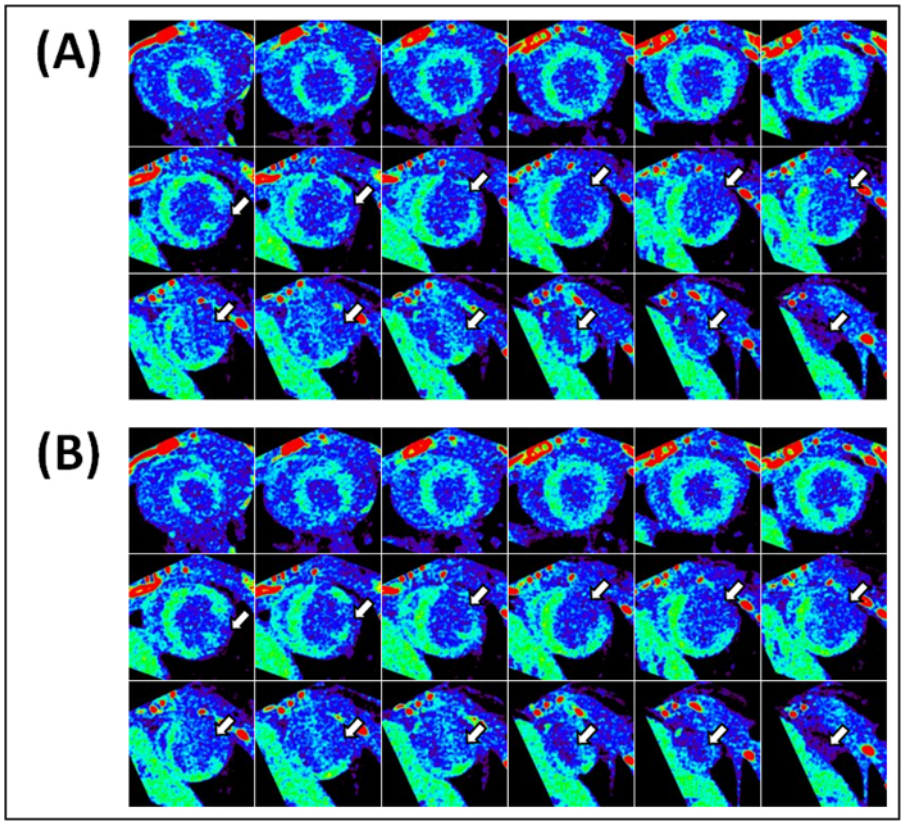

Figure 5. Representative metabolic uptake short-axial end-diastolic (**A**) and end-systolic (**B**) cross-sections of a mouse heart with myocardial infarction (Mouse 1). Images were acquired 6-7 hours after LAD coronary artery occlusion and 3-4 hr after contrast administration. The negative contrast noted by white arrows is due to lack of contrast metabolic uptake in the infarcted region.

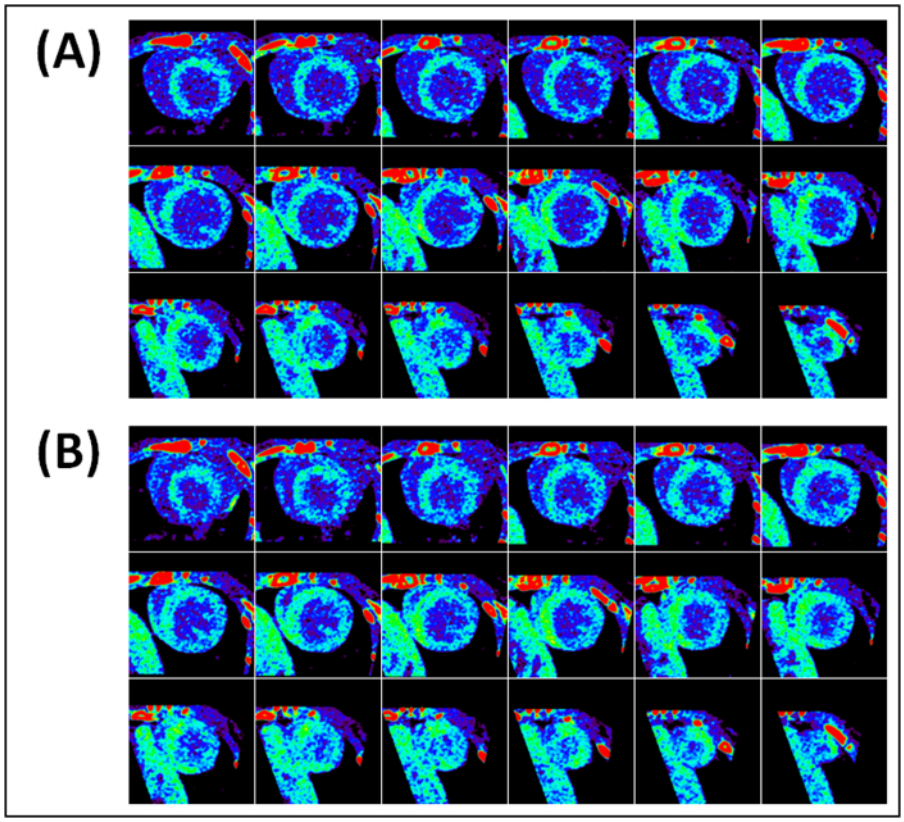

Figure 6. Representative metabolic uptake short-axial end-diastolic (**A**) and end-systolic (**B**) cross-sections of a mouse heart without myocardial infarction (Mouse 4). Images were acquired 6-7 hr after sham-operation and 3-4 hr after contrast administration. Myocardial metabolic uptake of contrast is uniformly present in all slices.

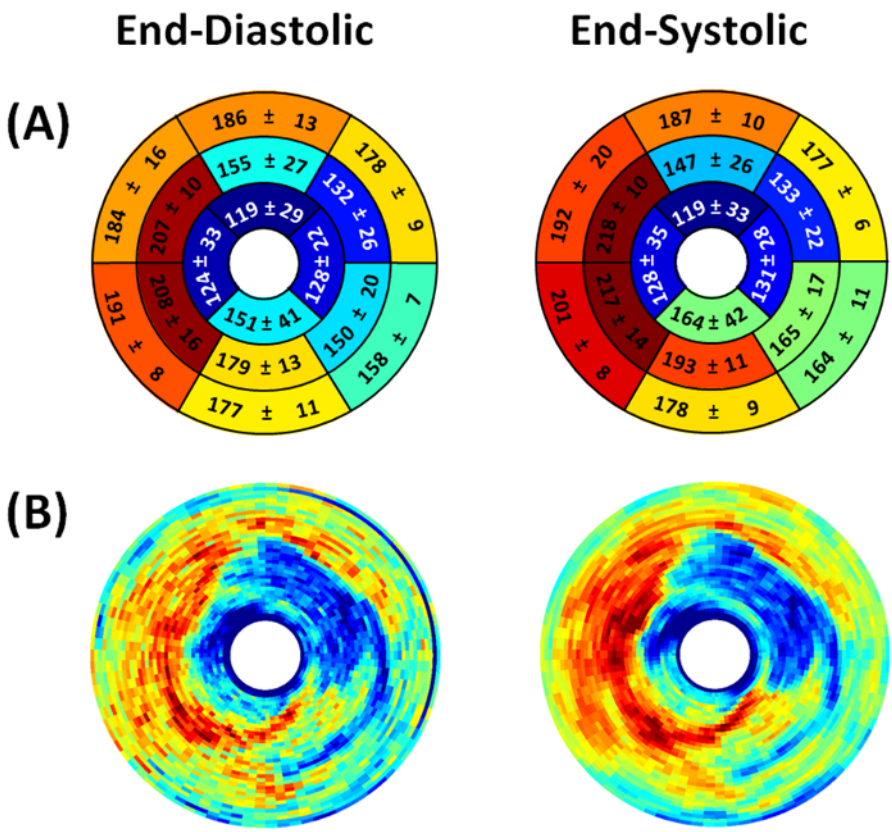

Figure 7. Representative end-diastolic and end-systolic circumferential polar plot displays (Bulls Eye polar plots) of myocardial metabolic uptake in a mouse with myocardial infarction. (**A**) The left ventricle is subdivided into basal, mid-cavity, and apical short-axial portions according to the 17-segment AHA model [25]. Dissimilar metabolic uptake is clearly visible in mid-anterolateral, apical anterior, apical inferior, and apical lateral segments. Values shown represent the segmental means in Hounsfield units ± standard deviations. (**B**) Myocardial metabolic uptake maps are shown without subdivision into 17 segments. The center of the plot corresponding to the cardiac apex (segment 17) is not shown.

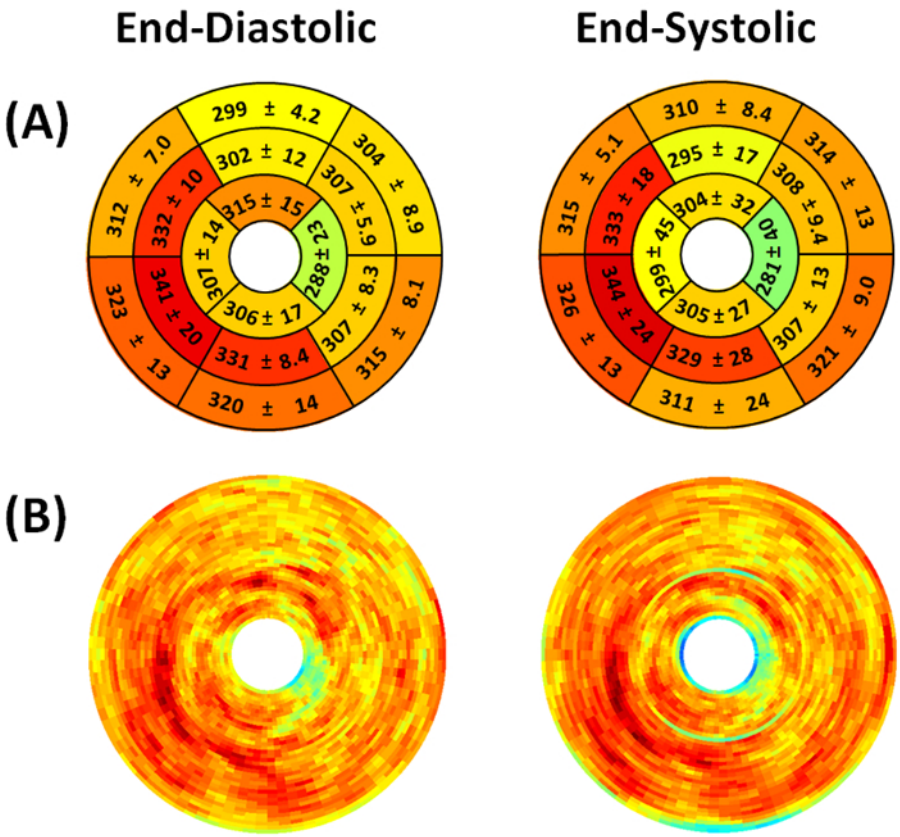

Figure 8. Representative end-diastolic and end-systolic circumferential polar plot displays (Bulls Eye polar plots) of myocardial metabolic uptake in a mouse without myocardial infarction. (**A**) The left ventricle is subdivided into basal, mid-cavity, and apical short-axial portions according to the 17-segment AHA model [25]. Dissimilar metabolic uptake is clearly visible in mid-anterolateral, apical anterior, apical inferior, and apical lateral segments. Values shown represent the segmental means in Hounsfield units ± standard deviations. (**B**) Myocardial metabolic uptake maps are shown without subdivision into 17 segments. The center of the plot corresponding to the cardiac apex (segment 17) is not shown.

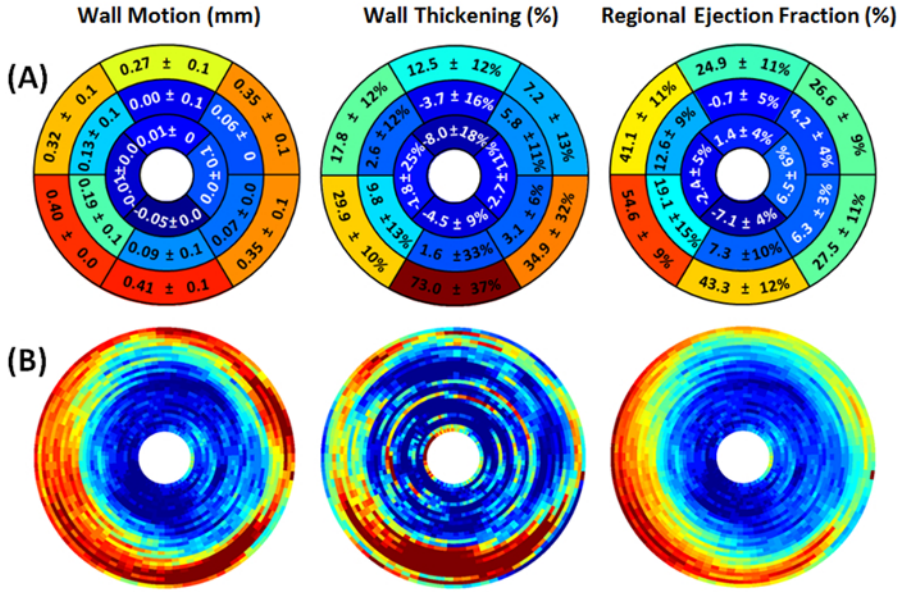

Figure 9. Representative myocardial wall motion (mm), wall thickening (%), and regional ejection fraction (%) circumferential polar plot displays (Bulls Eye polar plots) of a mouse with myocardial infarction. (**A**) The left ventricle is subdivided into basal, mid-cavity, and apical short-axial portions according to the 17-segment AHA model [25]. The presence of hypokinetic, akinetic, and dyskinetic regions in mid-cavity and apical portions denote extensive myocardial defect. (**B**) The regional myocardial measurement maps are shown without subdivision into 17 segments. The center of the plot corresponding to the cardiac apex (segment 17) is not shown.

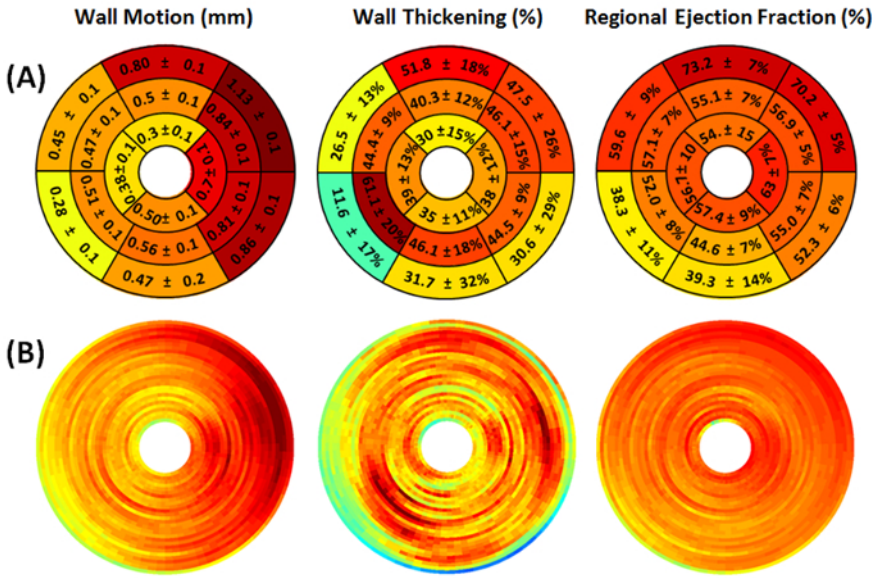

Figure 10. Representative myocardial wall motion (mm), wall thickening (%), and regional ejection fraction (%) circumferential polar plot displays (Bulls Eye polar plots) of a mouse without myocardial infarction. (**A**) The left ventricle is subdivided into basal, mid-cavity, and apical short-axial portions according to the 17-segment AHA model [25]. No apparent abnormality is detected. (**B**) The regional myocardial measurement maps are shown without subdivision into 17 segments. The center of the plot corresponding to the cardiac apex (segment 17) is not shown.

	Occluded LAD Artery				Sham
	Mouse 1	Mouse 2	Mouse 3	Mean ± SD	Mouse 4
Body Weight (g)	21.0	19.5	12.5	17.7 ± 4.5	25.0
Heart Rate (BPM*)	360	385	400	382 ± 20	395
LVEDV (µL)	61.22	48.60	35.98	48.6 ± 12.6	57.93
LVESV (µL)	51.87	36.59	25.42	37.9 ± 13.3	22.90
LVSV (µL)	9.35	12.01	10.56	10.6 ± 1.3	35.03
LVEF (%)	15.27	24.71	29.35	23.1 ± 7.1	60.47
CO (mL/min)	3.37	4.62	4.22	4.23 ± 0.4	13.84
$LVMV_{TOTAL}$	81.74	64.46	49.97	65.4 ± 16	99.75
LVMM (mg)	85.82	67.68	52.47	68.7 ± 17	104.74
LVMMI	4.09	3.47	4.20	3.9 ± 0.4	4.19
$LVMV_{MI}$ (µL)	18.34	8.57	7.88	11.6 ± 5.9	0.00
%LVMIS	22.44	13.30	15.77	17.7 ± 4.5	NA

Table 1. Left ventricular volumes and global functional indices measured in three mice 3 hours after LAD coronary artery occlusion and in a sham-operated mouse. *BPM, beats per minute; LVEDV, left ventricular end-diastolic volume; LVESV, left ventricular end-systolic volume; LVSV, left ventricular stroke volume; LVEF, left ventricular ejection fraction; CO, cardiac output; $LVMV_{TOTAL}$, total left ventricular myocardial volume; LVMM, left ventricular myocardial mass; LVMMI, left ventricular myocardial mass index; $LVMV_{MI}$, left ventricular myocardial infarction volume; %LVMIS, % left ventricular myocardial infarct size.

Discussion

Over the past several years MicroCT has become the modality many researches considered for characterization of cardiac structure and function in small animals[26-29,30]. However, the instrumentation used in the prior work was either custom built or no longer commercially available. As such, this study was aimed to provide a simple and comprehensive protocol for the use of high-speed MicroCT system with intrinsic cardio-respiratory gating to determine cardiac global and regional function along with myocardial perfusion and viability in small animals as models of human heart disease.

One of the most important requirements for studying heart structure and function is the scanner's ability to account for physiological heart movements. To this end, ECG-based prospective and retrospective gating techniques can be used. However, prospective (step and shoot) gating relies on a pre-specified interval of the cardiac cycle, for example during diastole, when the heart motion is least. With this approach only one image per cardiac cycle is obtained and only one phase of the cardiac cycle can be reconstructed. As such, in addition to being time consuming to generate, prospectively gated reconstructions produce only one dataset, which is deprived of functional information. Retrospective

gating, on the other hand, allows for reconstruction of multiple datasets at each portion of the cardiac cycle, thus allowing global and regional left ventricular functional analysis.

The current work employed cardiorespiratory reconstructions with intrinsic retrospective gating. Intrinsic retrospective gating utilizes proprietary image-based software to reconstruct end-diastolic and end-systolic cardiac phases without need for dedicated respiratory and cardiac monitoring devices[29,31,32]. An excellent agreement of intrinsic retrospective and extrinsic ECG-dependent retrospective gating for studying cardiac function in mice and rats was demonstrated by Dinkel *et al.*[29]. During this present work, intrinsic retrospective gating not only significantly minimized the time needed to set up the scan, but also eliminated dependency on monitoring hardware, such as ECG leads and respiratory pneumatic sensor, as well as additional operator skills to properly set it up.

Following the reconstruction, image quality of both end-diastolic and end-systolic datasets was found satisfactory for cardiac analysis. During examination of the images, particular attention was paid to motion artifacts that may occur during an inadequate level of anesthesia, streaking artifacts that can happen as a result of missing projections in animals with high respiration rate, low-attenuation artifacts that are commonly caused by bony structures and can mimic perfusion defects, and ring artifacts that can arise from mis-calibration or failure of one or more detector elements.

The ability of MicroCT to produce cardiac structural and functional information is also dependent on the availability of suitable intravascular contrast agent. Most currently commercially available MicroCT contrasts can be generally subdivided into particulate non-metabolizable macrophage specific and polydisperse metabolizable iodine-based contrasts[23,33-36]. Although particulate agents offer greater X-ray opacification due to their higher atomic number (barium, Z=56; and gold, Z=79), they cannot be used for metabolic assessment. Moreover, these agents are seen as noxious to the organism and removed by the liver macrophages (Kupffer cells), the scavenging cells of the reticuloendothelial system (RES). Because of their non-metabolizable nature, these agents induce changes to the liver microcirculation concomitant with liver damage[37].

Metabolizable iodine-based contrasts, on the other hand, are not targeted for RES-specific removal, thus should offer better safety profile and avoid liver toxicity. In addition to their better safety profile, these contrasts are taken up by metabolically active tissues, thus can be used for viability assessment[22,23]. To this end, iodinated contrast agent was selected for the present study. The contrast was administered at a dose of 5 or 10 µl per gram of animal body weight as a single bolus intravenous injection. Although both doses produced satisfactory enhancement results, a dose-dependent increase in left-ventricular and myocardial levels of contrast was observed when 10 µl/g of the contrast was injected. Of interest, with the larger dose, the duration of blood pool was prolonged and the peak of myocardial contrast uptake was delayed. One animal (Mouse 1) was followed up for 10 weeks after the surgery and during this period it was imaged every second week. From experience, no adverse effects related to the contrast (total of 5 injections) or related to X-ray exposure (total of 10 MicroCT scans) were observed in this mouse during the period of monitoring. One of the most commonly reported adverse effects of long-term iodine exposure is thyroid gland disturbance which was not observed macroscopically on post-mortem examinations. Mannheim *et al.* studied thyroxine levels after 3 consecutive contrast administrations and found no difference when the levels were compared to the controls[37]. With the use of the same MicroCT datasets, no signs of radiation-induced pulmonary fibrosis were detected in this animal (data not shown), conforming the safety of the procedure.

Assessment of global and regional ventricular heart function is considered the strongest determinant of cardiac performance and important in terms of prognosis and choice of therapeutic intervention[38,39]. The global left ventricular functional indices include left ventricular end-diastolic volume (LVEDV), left ventricular end-systolic volume (LVESV), left ventricular stroke volume (LVSV), left ventricular ejection fraction (LVEF), and cardiac output (CO). Earlier MicroCT studies confirmed that quantitative evaluation of global cardiac function is feasible in murine cardiovascular disease models and that pronounced decrease in global heart function takes place soon after LAD artery occlusion. These findings are in agreement with previous reports in that marked reduction in LVSV, LVEF, and CO occurred already on day 1 after occlusion[29,40-43]. It is noteworthy to mention that cardiac functional performance is dependent on the type and degree of anesthesia, thus for accurate measurements the heart rate during image acquisition should be kept as physiological as possible[44].

Quantitative assessment of left ventricular myocardial mass (LVMM) is important for evaluation of left ventricular hypertrophy and was primarily conducted using MRI[11,43,45,46]. LVMM is often corrected for body weight and presented as left ventricular myocardial mass index (LVMMI) to allow for normalization of cardiac weight among mice of different age and habitus. Accurate estimation of these parameters is important, as the mice with myocardial infarction develop significant LV hypertrophy[47]. Assessment of LVMM, LVMMI, and LV geometry is also important for diagnostics of cardiac hypertrophy and dysplasia[11]. As such, determination of these parameters will be additionally beneficial to differentiate conditions such as concentric hypertrophy, eccentric hypertrophy, or concentric remodeling. In the present work, both LVMM and LVMMI values were determined in mice subjected to LAD artery ligation and in the sham-operated animal. Subsequently, the size of myocardial infarction was identified and used to calculate the percentage of infarct size. Although during the surgery the ligature to the LAD coronary artery was applied at the same level, the occlusion generated infarcts with some variability: 13.3%, 15.8%, and 22.4% (**Table 1**). One possible explanation for this variability may emanate from differences in coronary artery anatomy and their territorial blood supply between the animals, and in agreement with previous reports[48]. The most common way of infarct size assessment in a mouse model of myocardial infarction is by *ex vivo* triphenyl tetrazolium chloride (TTC) staining, the technique that would not allow longitudinal monitoring of the disease in the same animal. In the context of earlier work by Ashton *et al.*[22] and of this present, it is noteworthy that MicroCT in conjunction with iodinated contrast agent can provide an alternative and non-destructive method of determining infarct size longitudinally.

An additional advantage of the MicroCT technique lies in the very accurate determination of regional ischemia. Like in humans the left coronary artery of the mouse splits into a descending artery (LAD) and a septal branch (LCX). However, in mice, the anatomy of the side braches of the LAD and LCX differs considerably between animals[48]. Large braches of the LCX sometimes closely parallel the LAD and since the coronary arteries of mice are intra-myocardial and therefore not visible, side braces of the LCX are at times accidently but unavoidably included in the coronary occlusion during the mouse-infarct procedure. As such, the circumferentional polar map obtained after MicroCT can be used to determine exactly which coronary arteries were occluded, since perfusion and contrast uptake in sectors 2, 3, 8 and 9 are affected by the LCX while sectors 7, 10, 11, 12, 13, 15, 16 and 17 are supplied by the LAD. Accordingly, the polar map is of great benefit for accurate determination of the occluded arteries and accordingly aids importantly in the correct interpretation of the effects of the myocardial infarction of cardiac function and disease progression.

The myocardial infarct mouse model used highly mimics the human clinical situation where coronary vessels become suddenly occluded as a result of an acute plaque rupture and is as such of great benefit to study the disease development of the infarcted heart[49]. While in the developed western countries treatment of patients suffering from myocardial infarction is aimed at quickly restoring recirculation of the coronary vessel, on many occasions, particularly in less economically developed countries where the incidence of myocardial infarction is rapidly increasing, the occlusion cannot be annulated in time[1,50]. This induces in large ventricular infarctions that most often will lead to chronic heart failure and are a tremendous burden on public health. Consequently, longitudinal non-invasive diagnostic methods using a myocardial infarct model with a permanent coronary artery occlusion and a large ventricular infarction are of great importance to develop new treatment strategies against this disease.

Myocardial CT perfusion imaging is a rapidly evolving technique that allows quantitative assessment of regional coronary blood flow abnormalities and their relevance to heart function and viability. Newer small animal studies reduced the gap between MicroCT and SPECT, the modality of choice for perfusion and viability assessment[22]. With the goal to evaluate the degree of regional blood flow impairment caused by the LAD coronary artery occlusion, the MicroCT data were also evaluated for myocardial perfusion information. The ligated LAD artery is known to provide blood supply to the free wall, part of the septum, and the apical region of the left ventricle. Myocardial perfusion defects (hypoenhanced areas) of mouse 1 are shown in a polar coordinate system and obvious in mid-anterior, mid-inferolateral, mid-anterolateral, apical anterior, and apical lateral segments, the findings are consistent with the same coronary distribution (**Figure 3**). No difference between perfusion defects derived from end-diastolic and end-systolic images was found in homosegments. The end-diastolic and end-systolic myocardial perfusion polar map displays of the sham-operated animal are shown in **Figure 4**. Slight differences in myocardial blood flow between the segments of the control animal are insignificant on both end-diastolic and end-systolic representations. Interestingly, the areas of hypoenhancement can be visually seen on short-axial cross-section images (**Figure 1**) and can be easily quantified as shown in **Figure 3**. This was not possible in the study by Befeda *et al.* and could be explained by greater noise of the MicroCT instrument used[22]. In order to be visually discerned, the signal differences must be at least three to five times greater than the noise (standard deviation) in the image[51]. Low noise of the MicroCT used in this study permitted detection of a small signal difference between impaired and normally perfused myocardium (127HU±23HU vs. 217HU±29HU), allowing successful assessment of myocardial perfusion pattern defects.

One of the major advantages of using iodinated contrast agent is the ability to assess myocardial viability and metabolism due to the contrast related myocardial enhancement. To our knowledge, the contrast's ability to enhance myocardium was first described by Detombe *et al.*[23] and its first use for myocardial infarction imaging was reported by Ashton *et al.*[22]. Although the group indicated that perfused myocardium in the mice with myocardial infarction showed enhancement similar to the controls, and that the infarcted myocardium showed no enhancement, quantitative assessment of the segmental myocardial enhancement was not reported. To further investigate whether myocardial enhancement can be quantitatively assessed, all the mice were reimaged using the same imaging protocol 3 - 4 hours after the contrast administration, when the myocardial enhancement relative to cavity was maximal.

Myocardial contrast uptake defects were visually observed on short-axial end-diastolic and end-systolic cross-section images of a mouse heart with myocardial infarction (**Figure 5**), but not in the sham-operated animal (**Figure 6**). Myocardial uptake was quantitatively assessed in each myocardial segment from both end-diastolic and end-systolic reconstructions and presented in a polar coordinate system (**Figure 7** and **8**). The end-diastolic and end-systolic homosegmental values obtained from the same animal were not different. However, the circumferential polar plots showed segment-specific abnormalities (**Figure 7**) with similar patterns as those shown on the myocardial perfusion maps (**Figure 2**). No contrast uptake defects were seen on the circumferential polar plots of the sham-operated mouse (**Figure 8**). The myocardial uptake data were of sufficient quality to perform global functional analysis and quantitative assessment of LV myocardial mass and infarct size (not shown). Although not pertinent to the currently used model with permanent LAD coronary artery occlusion, we believe that contrast myocardial extraction can be related not only to alterations in regional myocardial blood flow, but also to the status of cardiomyocytes (*e.g.* scarred, stunned and hibernating myocardium). To test this hypothesis, future work will employ the model with temporary myocardial ischemia and reperfusion.

Active contraction of myocardium results in myocardial wall motion and thickening which serve as important markers of systolic function and myocardial viability. Assessment of regional wall motion, thickening, and ejection fraction helps to discern passive systolic wall motion from active myocardial contraction. In order to enable standardized quantification of the extent and severity of the lesion, wall motion, wall thickening, and regional ejection fractions are commonly mapped into polar maps. Abnormalities of regional ventricular wall motion are important markers of myocardial ischemia that are most commonly assessed by MRI[52]. The LV wall motion, thickening and regional ejection fraction scores for each segment of a mouse with and without myocardial infarction are presented in **Figure 9** and **Figure 10**. As was expected, the LAD coronary artery ligation resulted in marked decrease of LV regional functional indices (**Figure 9**), whereas no effect was observed in the sham-operated mouse (**Figure 10**). These results are in concordance with previously reported data.

In conclusion, this work has demonstrated the first successful use of a high-speed MicroCT system for comprehensive determination of myocardial global and regional functional parameters along with assessment of myocardial perfusion and viability in healthy and in a mouse model of myocardial infarction. This work can be further extended towards characterization of other models of cardiovascular disease, allowing for accurate and non-destructive assessment of cardiac functional and pathophysiological changes, and for evaluation of novel preventive and therapeutic strategies.

Disclosures

E.D. van D., R. R., J. E. declare that they have no competing financial interests. S. B. is a paid employee of PerkinElmer, which manufactures the imaging instruments. Publication costs for this this video article were paid by PerkinElmer.

Acknowledgements

This work was supported by the stichting Lijf en Leven, project dilating versus stenosing arterial disease.

References

1. Finegold, J. A., Asaria, P., & Francis, D. P. Mortality from ischaemic heart disease by country, region, and age: statistics from World Health Organisation and United Nations. *Int J Cardiol.* **168**, 934-945 (2013).
2. Briaud, S. A. *et al.* Leukocyte trafficking and myocardial reperfusion injury in ICAM-1/P-selectin-knockout mice. *Am J Physiol Heart Circ Physiol.* **280**, H60-67 (2001).
3. Heymans, S. *et al.* Inhibition of plasminogen activators or matrix metalloproteinases prevents cardiac rupture but impairs therapeutic angiogenesis and causes cardiac failure. *Nat Med.* **5**, 1135-1142 (1999).
4. Kaijzel, E. L. *et al.* Multimodality imaging reveals a gradual increase in matrix metalloproteinase activity at aneurysmal lesions in live fibulin-4 mice. *Circ Cardiovasc Imaging.* **3**, 567-577 (2010).
5. MacLellan, W. R., & Schneider, M. D. Genetic dissection of cardiac growth control pathways. *Annu Rev Physiol.* **62**, 289-319 (2000).
6. Michael, L. H. *et al.* Myocardial ischemia and reperfusion: a murine model. *Am J Physiol.* **269**, H2147-2154 (1995).
7. Zhang, D. *et al.* TAK1 is activated in the myocardium after pressure overload and is sufficient to provoke heart failure in transgenic mice. *Nat Med.* **6**, 556-563 (2000).
8. Feldman, M. D. *et al.* Validation of a mouse conductance system to determine LV volume: comparison to echocardiography and crystals. *Am J Physiol Heart Circ Physiol.* **279**, H1698-1707 (2000).
9. Kolwicz, S. C., Jr., & Tian, R. Assessment of cardiac function and energetics in isolated mouse hearts using 31P NMR spectroscopy. *J Vis Exp.* (2010).
10. Kubota, T. *et al.* End-systolic pressure-dimension relationship of in situ mouse left ventricle. *J Mol Cell Cardiol.* **30**, 357-363 (1998).
11. Lorell, B. H., & Carabello, B. A. Left ventricular hypertrophy: pathogenesis, detection, and prognosis. *Circulation.* **102**, 470-479 (2000).
12. Pacher, P., Nagayama, T., Mukhopadhyay, P., Batkai, S., & Kass, D. A. Measurement of cardiac function using pressure-volume conductance catheter technique in mice and rats. *Nat Protoc.* **3**, 1422-1434 (2008).
13. Buckberg, G. D. *et al.* Some sources of error in measuring regional blood flow with radioactive microspheres. *J Appl Physiol.* **31**, 598-604 (1971).
14. Krueger, M. A., Huke, S. S., & Glenny, R. W. Visualizing regional myocardial blood flow in the mouse. *Circ Res.* **112**, e88-97 (2013).
15. Vivaldi, M. T., Kloner, R. A., & Schoen, F. J. Triphenyltetrazolium staining of irreversible ischemic injury following coronary artery occlusion in rats. *Am J Pathol.* **121**, 522-530 (1985).
16. Johnson, K. Introduction to rodent cardiac imaging. *ILAR J.* **49**, 27-34 (2008).
17. Buonincontri, G. *et al.* MRI and PET in mouse models of myocardial infarction. *J Vis Exp.*, e50806 (2013).
18. Respress, J. L., & Wehrens, X. H. Transthoracic echocardiography in mice. *J Vis Exp.* (2010).
19. Gao, S., Ho, D., Vatner, D. E., & Vatner, S. F. Echocardiography in Mice. *Curr Protoc Mouse Biol.* **1**, 71-83 (2011).
20. Stillman, A. E., Wilke, N., & Jerosch-Herold, M. Myocardial viability. *Radiol Clin North Am.* **37**, 361-378, vi (1999).
21. Lahoutte, T. Monitoring left ventricular function in small animals. *J Nucl Cardiol.* **14**, 371-379 (2007).
22. Ashton, J. R. *et al.* Anatomical and functional imaging of myocardial infarction in mice using micro-CT and eXIA 160 contrast agent. *Contrast Media Mol Imaging.* **9**, 161-168 (2014).
23. Detombe, S. A., Dunmore-Buyze, J., & Drangova, M. Evaluation of eXIA 160 cardiac-related enhancement in C57BL/6 and BALB/c mice using micro-CT. *Contrast Media Mol Imaging.* **7**, 240-246 (2012).
24. Prajapati, S. I., & Keller, C. Contrast enhanced vessel imaging using microCT. *J Vis Exp.* (2011).
25. Cerqueira, M. D. *et al.* Standardized myocardial segmentation and nomenclature for tomographic imaging of the heart. A statement for healthcare professionals from the Cardiac Imaging Committee of the Council on Clinical Cardiology of the American Heart Association. *Circulation.* **105**, 539-542 (2002).
26. Badea, C. T., Fubara, B., Hedlund, L. W., & Johnson, G. A. 4-D micro-CT of the mouse heart. *Mol Imaging.* **4**, 110-116 (2005).
27. Bartling, S. H. *et al.* Retrospective motion gating in small animal CT of mice and rats. *Invest Radiol.* **42**, 704-714, (2007).
28. Clark, D., Badea, A., Liu, Y., Johnson, G. A., & Badea, C. T. Registration-based segmentation of murine 4D cardiac micro-CT data using symmetric normalization. *Phys Med Biol.* **57**, 6125-6145 (2012).
29. Dinkel, J. *et al.* Intrinsic gating for small-animal computed tomography: a robust ECG-less paradigm for deriving cardiac phase information and functional imaging. *Circ Cardiovasc Imaging.* **1**, 235-243 (2008).
30. Drangova, M., Ford, N. L., Detombe, S. A., Wheatley, A. R., & Holdsworth, D. W. Fast retrospectively gated quantitative four-dimensional (4D) cardiac micro computed tomography imaging of free-breathing mice. *Invest Radiol.* **42**, 85-94, (2007).
31. Boileau, C. *et al.* TGFB2 mutations cause familial thoracic aortic aneurysms and dissections associated with mild systemic features of Marfan syndrome. *Nat Genet.* **44**, 916-921 (2012).
32. Kachelriess, M., Sennst, D. A., Maxlmoser, W., & Kalender, W. A. Kymogram detection and kymogram-correlated image reconstruction from subsecond spiral computed tomography scans of the heart. *Med Phys.* **29**, 1489-1503 (2002).
33. Boll, H. *et al.* Comparison of Fenestra LC, ExiTron nano 6000, and ExiTron nano 12000 for micro-CT imaging of liver and spleen in mice. *Acad Radiol.* **20**, 1137-1143 (2013).
34. Ford, N. L. *et al.* Time-course characterization of the computed tomography contrast enhancement of an iodinated blood-pool contrast agent in mice using a volumetric flat-panel equipped computed tomography scanner. *Invest Radiol.* **41**, 384-390, (2006).
35. Hainfeld, J. F., Smilowitz, H. M., O'Connor, M. J., Dilmanian, F. A., & Slatkin, D. N. Gold nanoparticle imaging and radiotherapy of brain tumors in mice. *Nanomedicine (Lond).* **8**, 1601-1609 (2013).
36. Willekens, I. *et al.* Time-course of contrast enhancement in spleen and liver with Exia 160, Fenestra LC, and VC. *Mol Imaging Biol.* **11**, 128-135 (2009).
37. Mannheim, J. G., Schlichthärle, T., Pichler, B.J. Possible toxicological side effects after *i.v.* administration of iodine CT contrast agents. *World Molecular Imaging Conference, Dublin.* P400. (2012).
38. White, H. D. *et al.* Left ventricular end-systolic volume as the major determinant of survival after recovery from myocardial infarction. *Circulation.* **76**, 44-51 (1987).
39. Sheehan, F. H. *et al.* Advantages and applications of the centerline method for characterizing regional ventricular function. *Circulation.* **74**, 293-305 (1986).

40. Nahrendorf, M. *et al.* High-resolution imaging of murine myocardial infarction with delayed-enhancement cine micro-CT. *Am J Physiol Heart Circ Physiol.* **292**, H3172-3178 (2007).
41. Sheikh, A. Y. *et al.* Micro-CT for characterization of murine CV disease models. *JACC Cardiovasc Imaging.* **3**, 783-785 (2010).
42. Young, A. A., Barnes, H., Davison, D., Neubauer, S., & Schneider, J. E. Fast left ventricular mass and volume assessment in mice with three-dimensional guide-point modeling. *J Magn Reson Imaging.* **30**, 514-520 (2009).
43. Young, A. A. *et al.* Reperfused myocardial infarction in mice: 3D mapping of late gadolinium enhancement and strain. *J Cardiovasc Magn Reson.* **8**, 685-692 (2006).
44. Roth, D. M., Swaney, J. S., Dalton, N. D., Gilpin, E. A., & Ross, J., Jr. Impact of anesthesia on cardiac function during echocardiography in mice. *Am J Physiol Heart Circ Physiol.* **282**, H2134-2140 (2002).
45. Dall'Armellina, E. *et al.* Improved method for quantification of regional cardiac function in mice using phase-contrast MRI. *Magn Reson Med.* **67**, 541-551 (2012).
46. Shapiro, E. P. Evaluation of left ventricular hypertrophy by magnetic resonance imaging. *Am J Card Imaging.* **8**, 310-315 (1994).
47. Michael, L. H. *et al.* Myocardial infarction and remodeling in mice: effect of reperfusion. *Am J Physiol.* **277**, H660-668 (1999).
48. Salto-Tellez, M. *et al.* Myocardial infarction in the C57BL/6J mouse: a quantifiable and highly reproducible experimental model. *Cardiovasc Pathol.* **13**, 91-97, (2004).
49. van Deel, E. D. *et al.* Extracellular superoxide dismutase protects the heart against oxidative stress and hypertrophy after myocardial infarction. *Free Radic Biol Med.* **44**, 1305-1313 (2008).
50. Forouzanfar, M. H. *et al.* Assessing the global burden of ischemic heart disease, part 2: analytic methods and estimates of the global epidemiology of ischemic heart disease in 2010. *Glob Heart.* **7**, 331-342 (2012).
51. Rose, A. The sensitivity performance of the human eye on an absolute scale. *J Opt Soc Am.* **38**, 196-208 (1948).
52. Befera, N. T., Badea, C. T., & Johnson, G. A. Comparison of 4D-microSPECT and microCT for murine cardiac function. *Mol Imaging Biol.* **16**, 235-245 (2014).